Light-driven dynamic Archimedes spirals and periodic oscillatory patterns of topological solitons in anisotropic soft matter

Angel Martinez[1,2] and Ivan I. Smalyukh[1,2,3,4,*]

[1]*Department of Physics, University of Colorado, Boulder, CO 80309, USA*
[2]*Liquid Crystal Materials Research Center, University of Colorado, Boulder, CO 80309, USA*
[3]*Department of Electrical, Computer, and Energy Engineering and Materials Science and Engineering Program, University of Colorado, Boulder, CO 80309, USA*
[4]*Renewable and Sustainable Energy Institute, National Renewable Energy Laboratory and University of Colorado, Boulder, CO 80309, USA*
[*] *ivan.smalyukh@colorado.edu*

Abstract: Oscillatory and excitable systems commonly exhibit formation of dynamic non-equilibrium patterns. For example, rotating spiral patterns are observed in biological, chemical, and physical systems ranging from organization of slime mold cells to Belousov-Zhabotinsky reactions, and to crystal growth from nuclei with screw dislocations. Here we describe spontaneous formation of spiral waves and a large variety of other dynamic patterns in anisotropic soft matter driven by low-intensity light. The unstructured ambient or microscope light illumination of thin liquid crystal films in contact with a self-assembled azobenzene monolayer causes spontaneous formation, rich spatial organization, and dynamics of twisted domains and topological solitons accompanied by the dynamic patterning of azobenzene group orientations within the monolayer. Linearly polarized incident light interacts with the twisted liquid crystalline domains, mimicking their dynamics and yielding patterns in the polarization state of transmitted light, which can be transformed to similar dynamic patterns in its intensity and interference color. This shows that the delicate light-soft-matter interaction can yield complex self-patterning of both. We uncover underpinning physical mechanisms and discuss potential uses.

OCIS codes: (160.3710) Liquid crystals; (160.4330) Nonlinear optical materials; (240.4350) Nonlinear optics at surfaces; (160.1190) Anisotropic optical materials.

References and Links

1. J. Wesfreid, H. Brand, P. Monneville, G. Albinet, and N. Boccara, eds., *Propagation in Systems far from Equilibrium* (Springer, 1988).
2. R. J. Field and M. Burger, eds., *Oscillations and Traveling Waves in Chemical Systems* (Wiley, 1985).
3. F. X. Witkowski, L. J. Leon, P. A. Penkoske, W. R. Giles, M. L. Spano, W. L. Ditto, and A. T. Winfree, "Spatiotemporal evolution of ventricular fibrillation," Nature **392**(6671), 78–82 (1998).
4. L. B. Smolka, B. Marts, and A. L. Lin, "Effect of inhomogeneities on spiral wave dynamics in the Belousov-Zhabotinsky reaction," Phys. Rev. E Stat. Nonlin. Soft Matter Phys. **72**(5), 056205 (2005).
5. J. Luengviriya, P. Porjai, M. Phantu, M. Sutthiopad, B. Tomapatanaget, S. C. Müller, and C. Luengviriya, "Meandering spiral waves in a bubble-free Belousov–Zhabotinsky reaction with pyrogallol," Chem. Phys. Lett. **588**, 267–271 (2013).
6. A. L. Belmonte, Q. Ouyang, and J.-M. Flesselles, "Experimental survey of spiral dynamics in the Belousov-Zhabotinsky reaction," Phys. II France **7**(10), 1425–1468 (1997).
7. N. Li, J. Delgado, H. O. González-Ochoa, I. R. Epstein, and S. Fraden, "Combined excitatory and inhibitory coupling in a 1-D array of Belousov-Zhabotinsky droplets," Phys. Chem. Chem. Phys. **16**(22), 10965–10978 (2014).
8. K. B. Migler and R. B. Meyer, "Spirals in liquid crystals in a rotating magnetic field," Physica D **71**(4), 412–420 (1994).

#231579 - $15.00 USD Received 2 Jan 2015; revised 4 Feb 2015; accepted 4 Feb 2015; published 12 Feb 2015

9. I. Jánossy, K. Fodor-Csorba, A. Vajda, and L. O. Palomares, "Light-induced spontaneous pattern formation in nematic liquid crystal cells," Appl. Phys. Lett. **99**(11), 111103 (2011).
10. C. Zheng and R. B. Meyer, "Thickness effects on pattern formation in liquid crystals in a rotating magnetic field," Phys. Rev. E Stat. Phys. Plasmas Fluids Relat. Interdiscip. Topics **55**(3), 2882–2887 (1997).
11. K. B. Migler and R. B. Meyer, "Solitons and pattern formation in liquid crystals in a rotating magnetic field," Phys. Rev. Lett. **66**(11), 1485–1488 (1991).
12. S. Nasuno, N. Yoshimo, and S. Kai, "Structural transition and motion of domain walls in liquid crystals under a rotating magnetic field," Phys. Rev. E Stat. Phys. Plasmas Fluids Relat. Interdiscip. Topics **51**(2), 1598–1601 (1995).
13. T. Frisch, S. Rica, P. Coullet, and J. M. Gilli, "Spiral waves in liquid crystal," Phys. Rev. Lett. **72**(10), 1471–1474 (1994).
14. J. Palacci, S. Sacanna, A. P. Steinberg, D. J. Pine, and P. M. Chaikin, "Living crystals of light-activated colloidal surfers," Science **339**(6122), 936–940 (2013).
15. L. Giomi, M. J. Bowick, X. Ma, and M. C. Marchetti, "Defect annihilation and proliferation in active nematics," Phys. Rev. Lett. **110**(22), 228101 (2013).
16. T. Sanchez, D. T. N. Chen, S. J. DeCamp, M. Heymann, and Z. Dogic, "Spontaneous motion in hierarchically assembled active matter," Nature **491**(7424), 431–434 (2012).
17. Y. Zhang, N. Zhou, N. Li, M. Sun, D. Kim, S. Fraden, I. R. Epstein, and B. Xu, "Giant volume change of active gels under continuous flow," J. Am. Chem. Soc. **136**(20), 7341–7347 (2014).
18. P. G. de Gennes and J. Prost, *The Physics of Liquid Crystals*, 2nd Ed. (Clarendon, 1993).
19. P. M. Chaikin and T. C. Lubensky, *Principles of Condensed Matter Physics* (Cambridge University, 2000).
20. A. Martinez, H. C. Mireles, and I. I. Smalyukh, "Large-area optoelastic manipulation of colloidal particles in liquid crystals using photoresponsive molecular surface monolayers," Proc. Natl. Acad. Sci. U.S.A. **108**(52), 20891–20896 (2011).
21. I. I. Smalyukh and O. D. Lavrentovich, "Anchoring-mediated interaction of edge dislocations with bounding surfaces in confined cholesteric liquid crystals," Phys. Rev. Lett. **90**(8), 085503 (2003).
22. N. Petit-Garrido, R. P. Trivedi, J. Ignés-Mullol, J. Claret, C. Lapointe, F. Sagués, and I. I. Smalyukh, "Healing of defects at the interface of nematic liquid crystals and structured Langmuir-Blodgett monolayers," Phys. Rev. Lett. **107**(17), 8163–8170 (2011).
23. N. Petit-Garrido, R. Trivedi, F. Sagués, J. Ignés-Mullol, and I. I. Smalyukh, "Topological defects in cholesteric liquid crystals induced by chiral molecular monolayer domains," Soft Matter **10**, 8163–8170 (2014).
24. P. J. Ackerman, Z. Qi, and I. I. Smalyukh, "Optical generation of crystalline, quasicrystalline, and arbitrary arrays of torons in confined cholesteric liquid crystals for patterning of optical vortices in laser beams," Phys. Rev. E Stat. Nonlin. Soft Matter Phys. **86**(2), 021703 (2012).
25. A. Martinez, M. Ravnik, B. Lucero, R. Visvanathan, S. Žumer, and I. I. Smalyukh, "Mutually tangled colloidal knots and induced defect loops in nematic fields," Nat. Mater. **13**(3), 258–263 (2014).
26. C. P. Lapointe, S. Hopkins, T. G. Mason, and I. I. Smalyukh, "Electrically driven multiaxis rotational dynamics of colloidal platelets in nematic liquid crystals," Phys. Rev. Lett. **105**(17), 178301 (2010).
27. Q. Liu, Y. Yuan, and I. I. Smalyukh, "Electrically and optically tunable plasmonic guest-host liquid crystals with long-range ordered nanoparticles," Nano Lett. **14**(7), 4071–4077 (2014).
28. P. Yeh and C. Gu, *Optics of Liquid Crystal Displays* (Willey, New York, 1999).
29. P.-Y. Wang, W. Lu, D. Yu, and R. G. Harrison, "Excitability and pattern formation in a liquid crystal Fabry-Perot interferometer," Opt. Commun. **189**(1-3), 127–134 (2001).
30. M. Büttiker and R. Landauer, "Nucleation theory of overdamped soliton motion," Phys. Rev. A **23**(3), 1397–1410 (1981).
31. F. Lonberg, S. Fraden, A. J. Hurd, and R. B. Meyer, "Field-induced transient periodic structures in nematic liquid crystals: the twist-Fréedericksz transition," Phys. Rev. Lett. **52**(21), 1903–1906 (1984).
32. M. E. McConney, A. Martinez, V. P. Tondiglia, K. M. Lee, D. Langley, I. I. Smalyukh, and T. J. White, "Topography from topology: photoinduced surface features generated in liquid crystal polymer networks," Adv. Mater. **25**(41), 5880–5885 (2013).

1. Introduction

Dynamics, pattern formation and other non-equilibrium processes in soft and biological matter attract a great deal of attention [1–7], especially when they are light-driven or field-controlled [8–13]. Beyond their fundamental importance in modeling similar processes in biology [1,2], e.g. in testing Turing-type theories of morphogenesis [1], they potentially can be used in non-equilibrium self-organization of composite materials with a large structural diversity and dynamic control by weak external stimuli. For example, specially designed light-responsive active colloids form so-called "living crystals" [14] while biologically derived active nematic liquid crystals (LCs) exhibit constant generation and annihilation of topological defects [15,16]. Examples of recently introduced light-driven non-equilibrium soft matter systems include arrays of Belousov-Zhabotinsky droplets and gels [7, 17]. In

#231579 - $15.00 USD Received 2 Jan 2015; revised 4 Feb 2015; accepted 4 Feb 2015; published 12 Feb 2015

thermotropic LCs similar to the ones used in displays [18,19], a large variety of dynamic patterns, including spiral waves, have been generated by rotating magnetic fields [8–13]. Interestingly, these patterns arise in the molecular alignment field, also called director field $\mathbf{n}(\mathbf{r},t)$ [18], which is tangent to the average direction of nanometer-sized elongated LC molecules that can exhibit patterns varying as a function of spatial coordinates and time. The characteristic length scales associated with the patterns can range from tens of micrometers to millimeters while characteristic timescales are larger than the typical millisecond LC realignment times [8, 19]. In this work, we demonstrate that a rich variety of dynamic LC alignment patterns can also emerge when driven by low-intensity microscope illumination or ambient light and when the thin quasi-two-dimensional LC film is in contact with a light-responsive azobenzene monolayer [20]. The physical underpinnings behind the appearance of thsese patterns are elucidated by considering complex changes of the polarization state of initially linearly polarized light traversing through twisted, birefringent LC films of different thickness, combined with the surface anchoring-mediated [19–21] coupling between this polarization and the easy axis orientation defined by the polarization-sensitive azobenzene monolayer [20]. The dynamic patterns within the LC's and azobenzene monolayer's orientational ordering are also mimicked by the similarly changing patterns of the polarization state of light after passing through the dynamically driven sample, as well as by patterns of light intensity and interference colors obtained by subsequently passing this light through a waveplate and a polarizer. The dynamic patterns of azobenzene molecular orientations within the monolayer significantly expands our abilities of controlling structural organization in such single-molecule-thick soft matter systems [22,23]. Spiraling wave and other observed types of dynamics of topological solitons expand the defect control capabilities beyond their patterning into time-independent arrays [24] and elaborate three-dimensional spatial structures [25]. Our system may allow for nematic colloidal dispersions with light-driven rotation and assembly of anisotropic nematic LC colloids [26] and nanoinclusions [27].

2. Experimental system, methods, and materials

The LC cells were constructed using different combinations of photo-responsive confining substrates [20] and also glass plates coated with either thin films of uniaxially rubbed polyimide (PI-2555, from Nissan Chemicals) [21,25] or with monolayers of N,N-dimethyl-N-octadecyl-3-aminopropyltrimethoxysilyl chloride (DMOAP) [24] (Fig. 1), providing light-controlled or static planar or perpendicular boundary conditions at the LC-substrate interfaces, respectively. To obtain the photosensitive self-assembled surface monolayer on the glass plates, we submerged them into a ~1wt.% solution of 2-(4-dimethylamino-phenylazo)-N-(3-triethoxysilane-propyl)-benzamide (DMR) [20] in toluene. This was done at an elevated temperature of 45°C for 90 min to facilitate surface bonding of the DMR molecules. This surface treatment was followed by a toluene rinse, allowing us to wash away the excess DMR, followed by blowing the substrates with dry nitrogen and curing at 115°C for two hours. The studied glass cells were formed using plates bound by epoxy mixed with monodisperse spherical spacers used to set the gap thickness. Nematic cells that exhibit complex photo-driven dynamic and static patterns can be constructed using two photo-responsive substrates or one such substrate combined with one coated with polyimide or DMOAP. In some cases, the cell substrates were spaced using 2-4 μm glass spheres mixed into an acetone-diluted epoxy that was cured after adjusting the glass plates to assure cell thickness uniformity, while in others we used no spacers at all to achieve spatially varying submicron cell gap thicknesses determined by flatness of the glass plates used for cell fabrication. Wedge cells with dihedron angles between the glass plates of the order of 1-3 degrees were also fabricated, in which case the spacers were applied only on one side of the cell. After adjusting the cell substrates, we seal two opposite edges of the cell with more epoxy. In the case where one of the plates is treated with polyimide, the edges parallel to the rubbing direction are sealed first. Once the epoxy has cured, we fill the cell via capillary

#231579 - $15.00 USD Received 2 Jan 2015; revised 4 Feb 2015; accepted 4 Feb 2015; published 12 Feb 2015

action with the thermotropic nematic 4-cyano-4'-pentylbiphenyl (5CB). To mitigate the aligning effects of flow, we heat the cell to the isotropic phase and then quench back to the nematic phase. The two remaining cell edges are then sealed as well. To characterize the cell thickness locally in LC cells with in-plane director alignment, we used a Berek compensator to first precisely determine the phase retardation of initially linearly polarized light after passing the LC layer and then calculate the cell thickness using this measured retardation and the known optical refractive index anisotropy of the LC, $\Delta n = n_e - n_o \approx 0.2$, at the wavelength of the used blue illumination light [20]. Here n_e and n_o are the extraordinary and ordinary refractive indices, respectively.

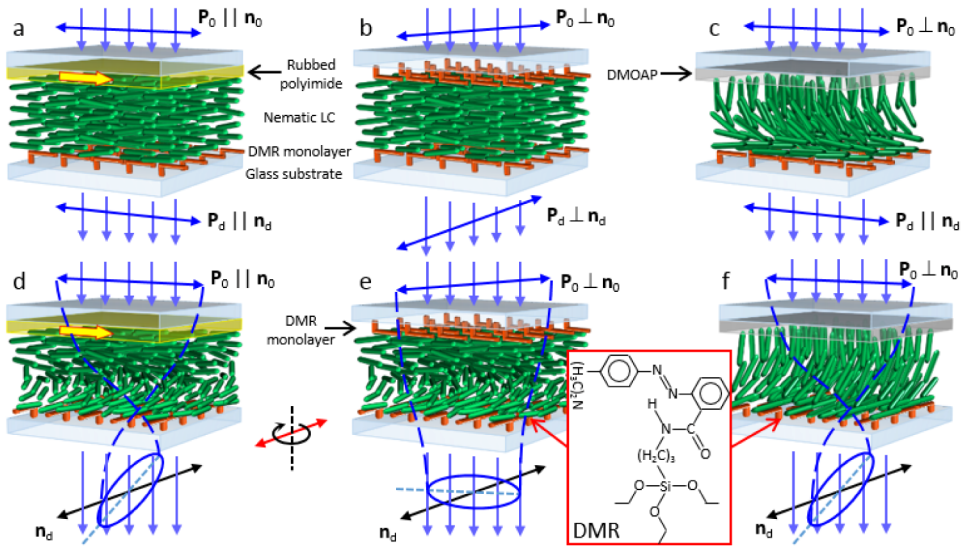

Fig. 1. Pattern-forming photo-responsive LC cell construction. (a-f) Three types of LC cells constructed with (a, d) one substrate coated with a film of rubbed polyimide (with easy axis along the yellow arrow) and another coated with a monolayer of the photo-responsive DMR, or (b, e) with both substrates coated with DMR, or (c,f) with one substrate coated with DMOAP to yield homeotropic anchoring and another coated with DMR. The cells are shown in two states: (a, b, c) at the first moment of illumination with linearly polarized blue light (along $\mathbf{P}_0$) and (d, e, f) in an evolved dynamic state sometime later when the second substrate is adaptively reorienting due to the photo-induced torque on $\mathbf{n}_d$ caused by polarized-light illumination, e.g. to drive $\mathbf{n}_d$ away from $\mathbf{P}_d$ in (a). The polarization of the output light is, in general, elliptical and oriented with its long axis at some angle with respect to the director at the output plane, $\mathbf{n}_d$. In the "dynamic equilibrium", the boundary condition $\mathbf{n}_d$ for the director at the exit substrate is constantly adjusted to be orthogonal to the long axis of the polarization ellipse orientation of which is dependent on the twist of director throughout the cell while this, in turn, adjusts the amount of director twist and, subsequently, further alters the polarization state, thus providing the nonlinear response and a feedback mechanism needed for the pattern formation.

Cells with dual DMR-treated confining glass plates can have any initial orientation with respect to the polarization of normally incident illumination light without affecting their ability of producing the studied dynamic patterns. However, cells containing one DMR-treated substrate and one plate coated with rubbed polyimide or DMOAP, in which the illumination light is necessarily incident from the side of DMOAP or polyamide coatings, introduce a complex dependence of the ensuing dynamic response with respect to this initial orientation, which we will discuss below.

For both driving and imaging of the dynamic patterns, we used an Olympus BX51 upright polarizing optical microscope with a coupled Spot 14.2 Color Mosaic Camera (Diagnostic Instruments, Inc.). The polarized imaging light source of a polarizing microscope itself is

#231579 - $15.00 USD Received 2 Jan 2015; revised 4 Feb 2015; accepted 4 Feb 2015; published 12 Feb 2015

used to generate most of the dynamic and static patterns presented in this study. Alternatively, we also used an illumination system consisting of a LC microdisplay with 1024x768 pixels (EMP-730, Epson) that controls transmitted light intensity on a pixel-by-pixel basis, as described in details elsewhere [20]. The used illumination patterns were generated using Microsoft PowerPoint. We used objective lenses of numerical aperture within 0.1-0.9 and with magnifications ranging from 2X to 50X. To avoid modification of the controlled $\mathbf{n}(\mathbf{r},t)$ patterns while imaging them by means of transmission-mode polarizing microscopy, we minimized exposure of samples by reducing exposure time and intensity while using maximum sensitivity of the Spot 14.2 Color Mosaic Camera and an optical filter that blocks the illumination light in the blue and violet ranges of the optical spectrum, to which the DMR is most sensitive. Cells with two DMR-coated substrates can be placed on the microscope's rotation stage with either substrate facing the light source (Fig. 1). The substrate through which the normally incident light passes first will be realigned to define an easy axis perpendicular to the linear polarization orientation (or, in general, to the major axis of the elliptical polarization state), while the far substrate interacts with the complex polarization field emerging after light is transmitted through the LC film containing nonuniform $\mathbf{n}(\mathbf{r},t)$. LC cells comprising one substrate coated with rubbed polyimide or DMOAP (Fig. 1), however, are oriented so that the illumination light passes through the LC-polyimide or LC-DMOAP interface first, before traversing the birefringent nematic medium and finally the photo-responsive DMR surface. To control the speed at which we drive the dynamic patterns, we tuned the intensity of white light while also adjusting the camera's sensitivity to avoid dark or saturated images. Alternatively, we also used broadband optical filters that block or transmit portions of the visible optical spectrum.

3. Results

3.1. Experimental characterization of dynamic patterns

When relatively thin LC cells (of thickness in the range d = 0.7-4 μm) are illuminated by blue, ultraviolet or white light, as depicted in Fig. 1, one observes rich dynamic behavior, with the most prominent dynamic pattern being the one shown in Fig. 2. This pattern has a visual resemblance of that seen in Belousov-Zhabotinsky reactions and also in homeotropic nematic cells driven by rotating magnetic fields [1–13]. Domains with different amounts and handedness of director twist across the cell thickness are separated by topological solitons in the form of Néel walls in orientations of DMR molecules and director at the LC-DMR interface, which penetrate into the LC bulk and appear as dark regions of a pattern shown in Fig. 2(a). By spatially tracking these inter-domain walls using ImageJ software and optical micrographs such as the ones presented in Fig. 2, we plot their coordinates at constant time [Figs. 3(a) and 3(b)]. A close examination reveals that, apart from the regions in the very centers of these patterns, our experimental data, presented in terms of cylindrical coordinates r versus θ for each of the two Néel wall arms, which appear as dark inter-domain spiraling stripes in the polarizing optical micrographs shown in Fig. 2(a), match the geometry of Archimedes spirals and can be fitted by a simple expression $r = r_0 + \Lambda\theta/(2\pi)$ [Fig. 3(b)]. Here Λ is the distance between consecutive solitons for a given spiral arm, which we call the "wavelength" of the dynamic topological pattern. By tracking the pattern's tip point, where the two arms of the spiraling Néel wall meet [Fig. 3(c)], based on videomicroscopy frames, we find that this point is meandering with time in the lateral plane of the cell, showing that the tips of spirals are not pinned to imperfections on substrates or dust inclusions. Furthermore, this meandering behavior [Fig. 3(c)] is qualitatively similar to that previously observed in the reaction diffusion oscillatory systems for geometrically similar Archimedes spiral dynamic patterns [5].

#231579 - $15.00 USD Received 2 Jan 2015; revised 4 Feb 2015; accepted 4 Feb 2015; published 12 Feb 2015

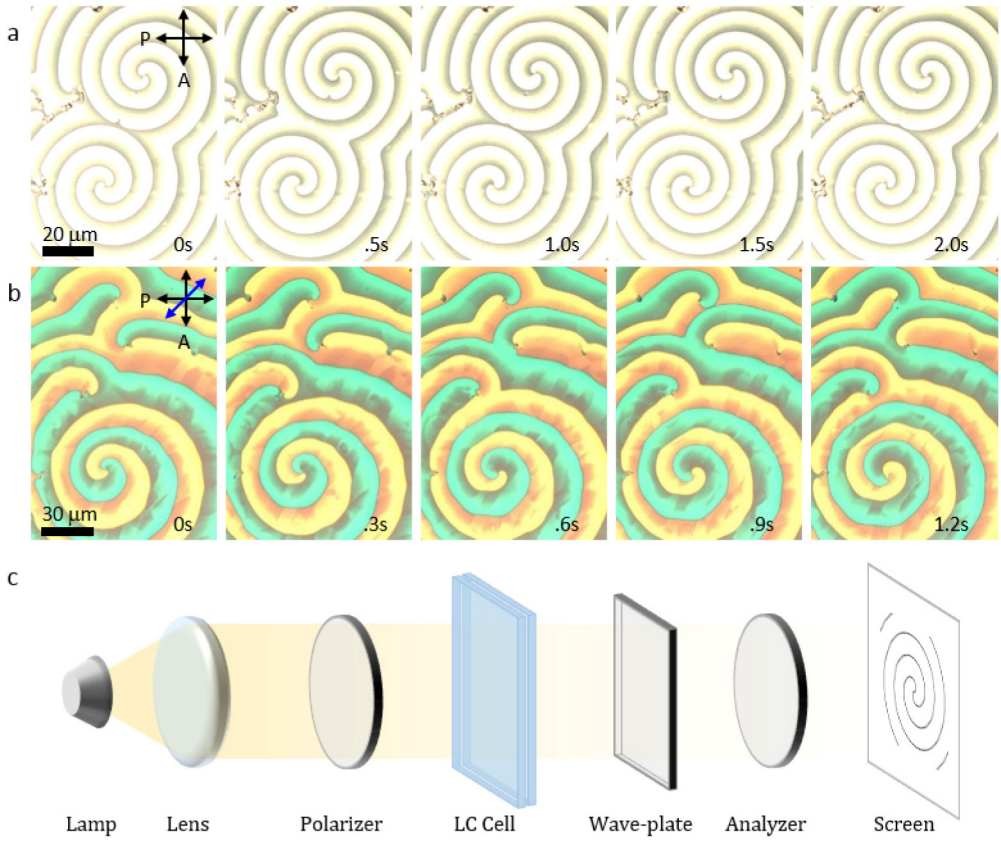

Fig. 2. Dynamic Archimedes spirals. (a, b) A series of polarizing micrographs extracted from a video, with elapsed time marked on them, for (a) two spiral patterns shown between crossed polarizers along black double arrows marked by "P" and "A" (Media 1) and (b) with an additional 530 nm wave-plate inserted between the polarizers and having the slow axis oriented along the blue double arrow (Media 2). The spiral arms in series (a) undergo 2π rotation over about 2 seconds while the spiral arms in series (b) undergo π rotation over about 1.2 seconds. (c) Schematic of the experimental setup.

The observed dynamic behavior of the Archimedes spirals is highly dependent on the intensity and spectral composition of the illumination light (Fig. 4). For example, white-light illumination in the polarizing microscope setting [Fig. 4(a)] yields a pattern rotation rate of ~0.37 Hz. This rate drops only slightly down to ~0.3 Hz as an absorptive color filter is inserted so that only blue light takes part in the sample illumination [Fig. 4(b)]. However, the pattern becomes static when the color filters are selected so that only red or longer-wavelength light participates in the sample illumination [Fig. 4(c)]. By controlling the intensity of white-light microscope illumination up to about 100 µW, the pattern rotation rate could be varied from 0 Hz (static pattern) to about 5 Hz. These observations are rather natural as the self-assembled DMR monolayers are photosensitive only in the blue-ultraviolet parts of the optical spectrum. We also find that the LC cells with DMR-DMR, polyimide-DMR, and also DMOAP-DMR alignment layers all yield similar dynamic self-patterning behavior (Fig. 1), although the details of patterns and conditions for their observations are somewhat different. This suggests that the light-matter interaction within the LC and at the exit substrate is responsible for the feedback mechanism typically associated with appearance of such dynamic patterns [1–13].

#231579 - $15.00 USD Received 2 Jan 2015; revised 4 Feb 2015; accepted 4 Feb 2015; published 12 Feb 2015

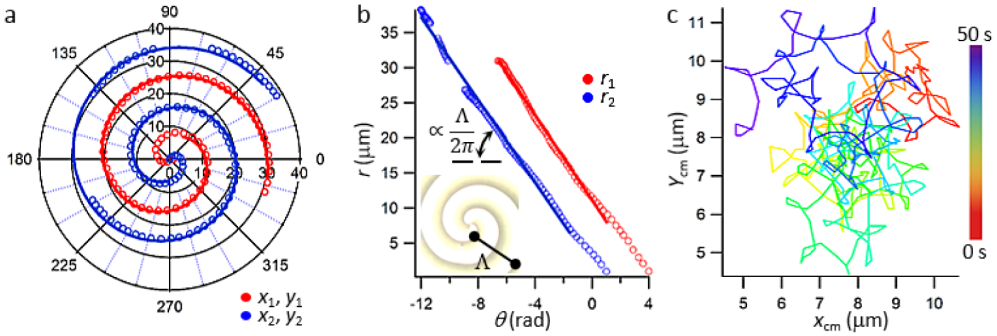

Fig. 3. Analysis of dynamic Archimedes spiral patterns in optically driven nematic cells. (a) A polar plot of the spiraling Néel wall coordinates in the r-θ cylindrical coordinate system at a constant time, as measured experimentally for the two spiral arms (red and blue filled circles). (b) Linear plots of r versus θ for each arm. The linear red and blue lines in (a,b) are fits of experimental data to an expression $r = r_0 + \Lambda\theta/(2\pi)$ defining the Archimedes spiral geometric configuration. The distance between consecutive solitons (wavelength) for a given spiral arm is denoted as Λ, and is defined in the inset of (b). The fits of two spiraling arms yield wavelengths Λ_1 = 19.03 μm and Λ_2 = 18.5 μm. (c) Coordinates of the "center of mass" of the spiraling pattern tracked over time and color-coded according to the time-color scale on the right to illustrate the meandering behavior similar to that of Archimedes spirals in chemical reaction diffusion systems.

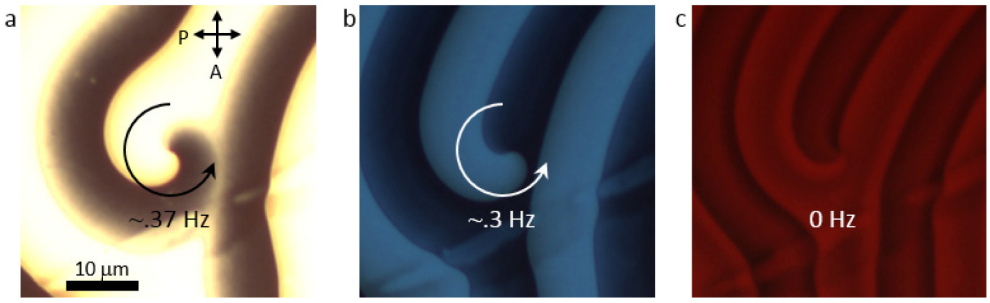

Fig. 4. Dependence of pattern dynamics on the color of illumination light. (a-c) Three frames of a single time series showing the dependence of defect dynamics on the color of illumination light (Media 3). (a) The pattern is driven by white microscope light at a rate of ~0.37 Hz. (b) the pattern is also effectively driven by blue light to which DMR is highly sensitive, although the rate decreases slightly upon insertion of a blue color filter due to the decreased overall intensity. (c) An optical micrograph showing a static pattern obtained upon insertion of a red color filter: since the interaction of the DMR with red light is negligible, the initially dynamic pattern "freezes" under red illumination. The crossed polarizers are oriented along black double arrows marked by "P" and "A" in (a) and rotation rates are marked on images.

As the cell thickness is varied, e.g. by means of producing wedge-shaped LC cells, the variety of observed dynamic and static patterns greatly increases (see micrographs in Fig. 5 and the videos linked to them) and includes various periodic or quasi-periodic arrays of circular and linear stripe-like domains. Some of the patterns, which are initially dynamic, can become static with time. For example, the stripe-like pattern shown in Figs. 5(e) and 5(f) has domains with static horizontally oriented stripes and also dynamic vertically oriented stripes. In this particular case, the dynamic stripes are gradually replaced by the horizontal static ones and the entire pattern eventually becomes static. However, this is not the case for all other types of patterns that we observed as they keep exhibiting different forms of dynamic behavior as long as the illumination light is on, or even in ambient light.

#231579 - $15.00 USD Received 2 Jan 2015; revised 4 Feb 2015; accepted 4 Feb 2015; published 12 Feb 2015

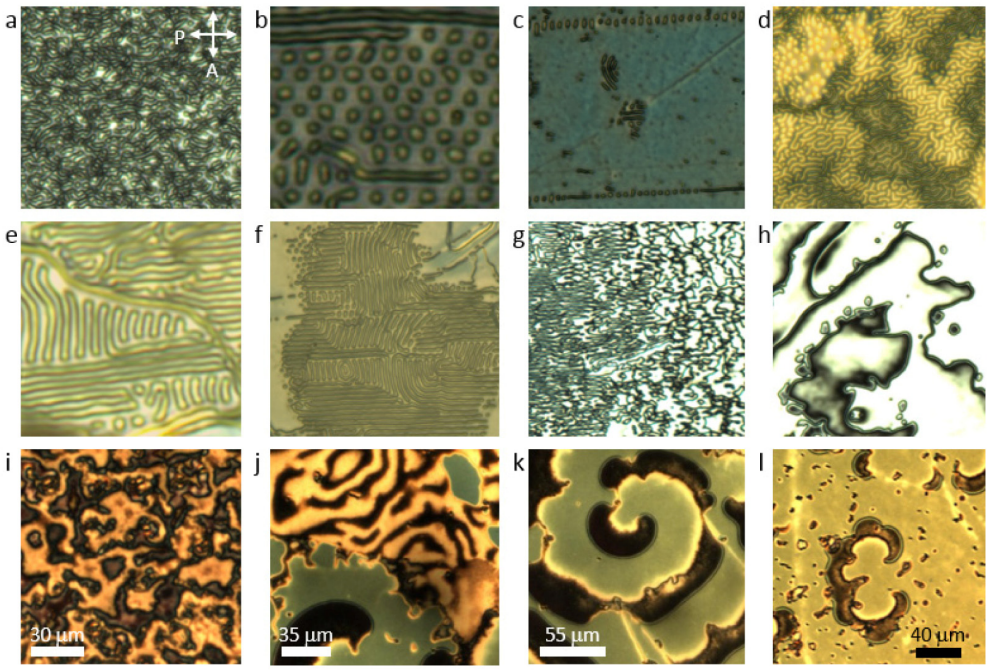

Fig. 5. Summary of dynamic and static patterns in addition to the propagating Archimedes spiral waves. (a-l) Twelve examples of different species of observed dynamic patterns, all driven with linearly polarized white light and viewed between crossed polarizers oriented along the image edges (Media 4, Media 5, Media 6, Media 7, Media 8, Media 9, Media 10, Media 11, Media 12, Media 13, Media 14, and Media 15). The patterns (a-g) arise in thinner cells of thickness d = 1-2 µm while the patterns (h-l) are observed in thicker cells of d = 2-4 µm.

3.2. Modeling of feedback mechanisms

To obtain insights into the underlying physics responsible for the observed dynamic patterns, as an example, we consider an initially planar LC cell with the DMR-LC interfaces at both confining substrates, as depicted in Fig. 1(b). The direct coupling of the electric field of illumination light and the LC director in the bulk of our cells can be neglected as the used intensities are many orders of magnitude lower than what is needed for the optical Fréedericksz transition [18,20,24,28,29]. At the surfaces, however, the illumination light sets the polarization-sensitive boundary conditions with the director's easy axis orientations orthogonal to the linear polarization direction or to the major axis of the polarization ellipse. As the linearly polarized light illuminates the first DMR-LC interface at $z = 0$, it sets the easy axis orientation $\mathbf{n}_0(x,y) = \mathbf{n}(x,y,z = 0)$ to be orthogonal to the initial linear polarization direction $\mathbf{P}_0$. However, it is also important to note that, due to finite intensity-dependent surface anchoring $W_0(I)$, the director can be forced to rotate away from this easy axis orientation. In the case where the initial director orientation across the cell and DMR orientations within the two monolayers at confining substrates happen to be uniform and orthogonal to $\mathbf{P}_0$, no patterns develop. However, this is rarely the case as the director and DMR molecular ordering is multi-domain upon cell preparation and after quenching the LC from isotropic to nematic phase. Although the linearly polarized illumination light sets uniform planar boundary conditions at the entrance surface $\mathbf{n}(x,y,z = 0)$, its action on the DMR and the easy axis for director $\mathbf{n}(x,y,z = d)$ depends on how the polarization of light changes during its propagation within the LC film. As the initially linearly polarized light traverses through the LC cell, its polarization is altered by the LC medium due to birefringence and the director (optical axis) twist across the cell. Generally, the outgoing light

#231579 - $15.00 USD Received 2 Jan 2015; revised 4 Feb 2015; accepted 4 Feb 2015; published 12 Feb 2015

is elliptically polarized (Fig. 1), with the azimuthal orientation, ψ, of the major axis of the polarization ellipse measured relative to the orientation of the director at the second LC-DMR interface, $\mathbf{n}_d(x,y,t) = \mathbf{n}(x,y,z = d,t)$; both ψ and elipticity ε are dependent on the LC film thickness as well as director twist across the cell (Fig. 6). This causes a nontrivial interplay between the polarization of the outgoing light, $\mathbf{P}_d$, with $\mathbf{n}_d(x,y,t)$. Furthermore, dynamic changes of $\mathbf{n}_d(x,y,t)$ in response to changes of the polarization state of outgoing light lead to changes of director structure across the cell thickness and thus further alter the polarization state itself, providing the nonlinear response and a feedback mechanism that is key to understanding the observed dynamic patterns.

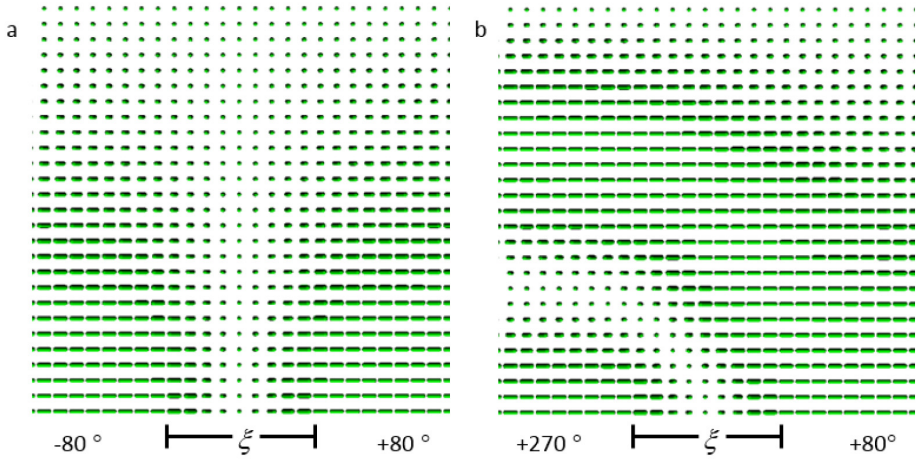

Fig. 6. Director structure of the inter-domain solitonic Néel wall regions. (a) Numerically simulated equilibrium director field configurations corresponding to the inter-domain pattern regions with different directions of ± 80° twist. (b) Computer-simulated director field configurations corresponding to the inter-domain regions with different 270° and 80° twist across the cell. The field configurations correspond to initially dynamic patterns that are "frozen" by removing blue and ultraviolet components of illumination light, as in the example shown in Fig. 4(c).

The total light's polarization-dependent surface anchoring (LPDSA) free energy at the two confining surfaces [Figs. 1(b) and 1(d)] can be written as

$$F_{\mathrm{LPDSA}} = [W_0(I)/2]\int (\mathbf{P}_0 \cdot \mathbf{n}_0)^2 dS + [W_d(I,\varepsilon)/2]\int (\mathbf{P}_d \cdot \mathbf{n}_d)^2 dS, \qquad (1)$$

where $W_0(I)$ and $W_d(I,\varepsilon)$ are the light intensity and polarization dependent surface anchoring coefficients at the two confining surfaces; the positive sign in front of this term indicates that they are minimized when the easy axes $\mathbf{n}_0$ and $\mathbf{n}_d$ are orthogonal to the linear or elliptical polarization major axis directions at these two planes, $\mathbf{P}_0$ and $\mathbf{P}_d$, respectively [Figs. 1(b) and 1(e)]. The LPDSA-driven director distortions are resisted by the bulk elastic free energy describing the energetic cost of director distortions [18,19]

$$F_{\mathrm{elastic}} = \int \left\{ \begin{array}{l} \frac{K_{11}}{2}(\nabla \cdot \mathbf{n})^2 + \frac{K_{22}}{2}[\mathbf{n} \cdot (\nabla \times \mathbf{n}) + \frac{2\pi}{p}]^2 + \frac{K_{33}}{2}[\mathbf{n} \times (\nabla \times \mathbf{n})]^2 \\ -K_{24}[\nabla \cdot [\mathbf{n}(\nabla \cdot \mathbf{n}) + \mathbf{n} \times (\nabla \times \mathbf{n})]] \end{array} \right\} dV, \qquad (2)$$

where K_{11}, K_{22}, K_{33}, and K_{24} are Frank elastic constants for splay, twist, bend and saddle splay director deformations, respectively. The competition of corresponding LPDSA and bulk elastic torques guides dynamics of the system that can be described by a dynamical equation for the LC director [18]:

#231579 - $15.00 USD Received 2 Jan 2015; revised 4 Feb 2015; accepted 4 Feb 2015; published 12 Feb 2015

$$\Gamma_v = \mathbf{n} \times \frac{\delta F}{\delta \mathbf{n}}, \tag{3}$$

Where Γ_v is the corresponding viscous torque and $F = F_{\text{elastic}} + F_{\text{LPDSA}}$. For simplicity, we can assume that the backflow effects can be neglected and that the viscous torque is proportional to the angular velocity of the director about an axis perpendicular to itself [18, 19]:

$$\Gamma_v = -\gamma_1 \left(\mathbf{n} \times \frac{\partial \mathbf{n}}{\partial t} \right). \tag{4}$$

In the studied light-induced patterns, director twist distortions are the most abundant, although other types of deformations are present in-between the domains of different direction and amount of twist. Within the uniformly twisted domains, the changes of polarization of light can be modeled both analytically and numerically using a Jones matrix approach [28], similar to that used in modeling of twisted nematic displays. At sufficiently large intensities of illumination, one can assume that the anchoring coefficient $W_0(I)$ is relatively large and the boundary conditions at the first DMR-LC interface prescribe that $\mathbf{n}_0 \perp \mathbf{P}_0$. This assures the selection of the ordinary mode of incident light at the entrance of the LC cell with DMR-DMR photoalignment monolayers, yielding, in general, an elliptically polarized outgoing light [Fig. 1(e)] with the polarization state characterized by [28]:

$$\varepsilon = \tan\left(\frac{1}{2} \sin^{-1}\left[-\frac{\Omega\phi}{X^2} \sin^2 X \right] \right) \tag{5}$$

$$\tan 2\psi = \frac{2\phi X \tan X}{X^2 - \left(\phi^2 - \Omega^2/4\right)\tan^2 X}, \tag{6}$$

Where $X = (\phi^2 + \Omega^2/4)^{1/2}$, $\Omega = 2\pi\,(n_e - n_o)d/\lambda$, λ is the central wavelength of the illumination light, the elipticity ε is defined as the ratio of the minor and major axes of the polarization ellipse, and ϕ is the director twist angle across the cell of thickness d. The analysis of these equations reveals a rich behavior as a function of cell thickness, optical anisotropy of the LC, as well as the overall twist across the cell. This richness of altering the outgoing light's polarization state is responsible for the ensuing richness of feedback mechanisms and the large variety of observed dynamic patterns (Figs. 2-5). A regime of particular interest is when the rotation of the long axis of ellipse upon exiting the cell is lagging the corresponding rotation of the LC director, which is similar to the case of a rotating magnetic field and director rotation in magnetically induced dynamic patterns [8, 10–13] and corresponds to the dynamic Archimedes spiral patterns (Figs. 2 and 3). To obtain a rough qualitative description of the observed pattern dynamics, we (a) disregard the K_{24}-term of elastic free energy, (b) adopt the one elastic constant approximation with $K = K_{11} = K_{22} = K_{33}$, (c) assume that the surface anchoring at LC-DMR interface is infinitely strong so that the first term in Eq. (1) can be disregarded, as well as (d) introduce the characteristic director relaxation time of director rotation in response to the change of an easy axis orientation at the $z = d$ LC-DMR interface, $\tau = 2\gamma_1/W_d(I,\varepsilon)$, and the surface anchoring extrapolation length, $\xi = K/W_d(I,\varepsilon)$. Despite qualitative similarities, due to a complicated feedback mechanism arising through the dynamically changing polarization states of outgoing light altered by changes in the twisted LC director structure, our system is much more complex as compared to the case of pattern formation in a rotating magnetic field [8, 10–13]. However, the experiments show that the frequency characteristic of the Archimedes spiral pattern is roughly constant in time (Fig. 2). The analysis of Eqs. (5) and (6) reveals that the orientation of the long axis of polarization ellipse at the output plane of a relatively thin cell in this case can be lagging the director by an angle α, similar to the case where the director slightly lags behind the rotating magnetic field

#231579 - $15.00 USD Received 2 Jan 2015; revised 4 Feb 2015; accepted 4 Feb 2015; published 12 Feb 2015

in the studies of field-driven dynamic patterns. In analogy with Ref [8], we can therefore write a simplified torque balance equation in the following form:

$$\xi^2 \nabla \alpha - \tau \frac{\partial \alpha}{\partial t} + \omega\tau - \sin(2\alpha) = 0. \quad (7)$$

For the lateral dimensions of the pattern much larger than ξ and d, both about one micron or smaller, which is the case in our experiments (Fig. 2), one can re-write Eq. (7) as an equation for a traveling wave $\alpha = \alpha(r - v_w t)$, where v_w is the wave velocity:

$$\xi^2 \tau \frac{\partial^2 \alpha}{\partial^2 r} + v_w \tau \frac{\partial \alpha}{\partial r} + \omega\tau - \sin(2\alpha) = 0. \quad (8)$$

Previous studies [8,13,30,31] showed that Eq. (8) contains stable propagating wave solutions that can describe Archimedes spiral dynamic patterns similar to the ones observed in our experiments (Figs. 2 and 3). By extending this analysis to different LC cell thicknesses, which translates to a broad spectrum of polarization states accessed by light traversing through the twisted birefringent LC films, one can also understand the origin of a large variety of dynamic and static patterns that form in this system (Figs. 2-5).

3.3. Wall structure in the pattern

The studied dynamic patterns contain domains with different directionality and different amounts of twist across the cell thickness. At the interface of the LC and light-controlled self-assembled monolayer, the director and DMR molecules smoothly transition between the different orientations in the neighboring domains within a "Néel wall" soliton region of width expected to be comparable to the surface anchoring extrapolation length $\xi = K/W_d(I,\varepsilon)$ [18]. The estimate of this width based on experimental images (Figs. 2 and 4), yields submicron or about one micron values, consistent with the ratio of an average elastic constant K~10 pN and azimuthal surface anchoring coefficient for DMR monolayers $W_d(I,\varepsilon) \sim 10^{-4}$-$10^{-5}$ J/m^2 [20]. To gain insights into the structure of the inter-domain solitonic configurations, which are commonly referred to as Néel walls in analogy with magnetism [19], we have performed computer simulations of detailed director structures in the inter-domain regions through minimization of free energy F (Fig. 6). Since the domain width is 50-100 times larger than the cell thickness d and the extrapolation length ξ, both ~1 μm or even smaller in the case of Archimedes spiral patterns, we focus on one inter-domain region between domains of different twist (Fig. 6) while neglecting its interaction with the other solitonic domain walls. The static field configurations that correspond to micrographs like the one shown in Fig. 4(c), when a dynamic pattern becomes "frozen" in time due to eliminating blue and ultraviolet spectral components of light illumination, are obtained by minimizing the free energy using the so-called director relaxation method for static boundary conditions on confining substrates and far from the inter-domain region. The analysis of elastic free energy density associated with the minimum-energy field configurations reveals that the most energetically costly parts of the structure correspond to near-surface regions in-between the differently twisted domains (Fig. 6), within the solitonic structures between the domains with the same amount but different directionality of twist [Fig. 6(a)] and the ones with same directionality but different amount of twist across the cell [Fig. 6(b)]. Although the structure of the inter-domain dynamic walls is not necessarily corresponding to the minimum elastic energy, as the structure of Archimedes spiral and other dynamic patterns never arrive to the equilibrium, these simulated field configurations describe their static versions obtained by turning off the blue and ultraviolet components of the illumination light [as in the example of Fig. 4(c)] and provides insights into energetics involved in the dynamic pattern formation, and also may correspond to the static domain patterns such as the horizontal stripes shown in Figs. 5(e)-5(g).

#231579 - $15.00 USD Received 2 Jan 2015; revised 4 Feb 2015; accepted 4 Feb 2015; published 12 Feb 2015

3.4. Effects of surface boundary conditions and lateral confinement

To uncover the elements of geometry of our photo-responsive system that are essential to observe dynamic patterns, in addition to the DMR-DMR photoalignment geometry discussed above [Figs. 1(b) and 1(e)], we have also studied cells with hybrid (homeotropic-planar) DMOAP-DMR [Figs. 1(a) and 1(d)] and planar rubbed polyimide–DMR confining surfaces [Figs. 1(c) and 1(f)]. We find that the dynamic patterns are still observed for the majority of incident linear polarization states, as long as the incident light is passed through the photoresponsive substrate after first traversing through the homeotropic or polyimide-coated confining surface and the LC film. The dynamic patterns are also robust with respect to various types of lateral confinement of the illuminated region within the plane of the LC cell (Fig. 7), although this lateral confinement is influencing selection of different dynamic pattern modes in the LC cells. To test the possible role of lateral confinement, we were driving patterns by blue or white light illumination with total power of about 100 μW derived from a projection system [20] while imaging the ensuing dynamic-self-patterning in red light (Fig. 7) to which the DMR photoalignment layers are insensitive. We find that no self-patterning takes place in the hybrid DMOAP-DMR and polyimide-DMR cells when the polarization direction of the square-shaped blue-light illumination region is orthogonal to the $\mathbf{n}_d$ in the output plane and also the director across the entire cell thickness [Figs. 1(a), 1(d), 1(c), and 1(f)]. However, once this linear polarization of illumination light is rotated in an arbitrary direction for a short period of time, a wide variety of patterns can form with their structural features and dynamics highly sensitive to the details of the pattern initiation process. This observation again appears to be consistent with the mechanisms of nonlinearity and feedback in the response of our system that lead to the studied dynamic self-patterning. Finally, it is interesting that the DMOAP-DMR hybrid cells with the geometry shown in Figs. 1(c) and 1(f) host dynamic patterns with time-varying director field configurations that are essentially half of those seen in magnetically induced dynamic patterns studied previously [8, 10–13].

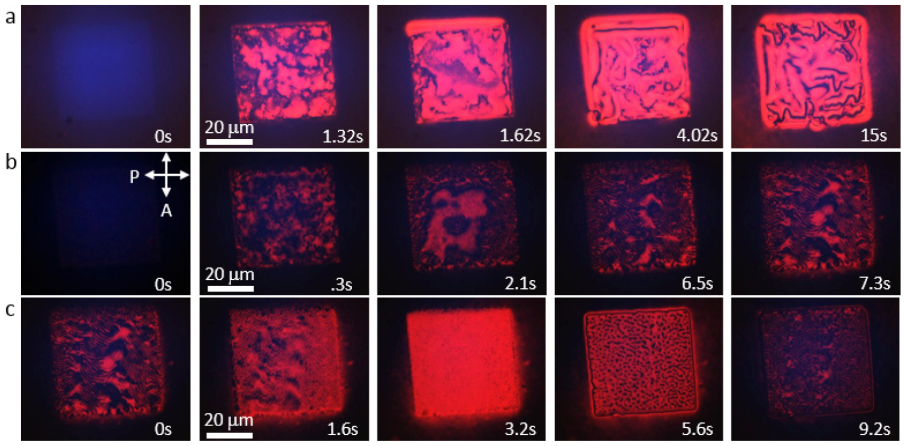

Fig. 7. Dynamic light-driven patterns in hybrid DMOAP-DMR wedge cells in presence of lateral confinement of the illuminated area. (a-c) Square regions illuminated with linearly polarized blue light viewed between crossed polarizer and analyzer oriented along white double arrows marked with "P" and "A" in (b) (Media 16, Media 17, and Media 18). Time series (a) shows an illuminated region at the thick side of the wedge-shaped cell (d≈4 μm), while the frame series (b) and (c) are obtained in a cell region at the thin side (d≈1 μm). Series (a) and (b) show the illuminated cell region during successively evolved states (with elapsed time marked on the frames extracted from a video) under constant illumination. The transformation of dynamic patterns shown in (c) was initiated by a π-rotation of the linear polarization of incident light beginning from the orientation of this linear polarization $\mathbf{P}_0$ along the vertical edge of the corresponding video frames.

#231579 - $15.00 USD Received 2 Jan 2015; revised 4 Feb 2015; accepted 4 Feb 2015; published 12 Feb 2015

4. Discussion

Although pattern formation, including Archimedes-spiral-like patterns, due to laser beams in the experimental setting of LC Fabry-Perot interferometers is known [29], it commonly requires a special setup design and laser powers of the order of tens of milliwatts. A distinctive feature of our system is that even low-intensity ambient light can induce such pattern formation. Interestingly, in twisted nematic cells, the optical Fréedericksz threshold intensity for director realignment is typically orders of magnitude greater as compared to homeotropic LC cells [20,28], which is due to the complex interplay between the polarization state of light propagating in the twisted birefringent LC, such as the linear polarization's Mauguin following of the director twist [18], and its coupling to the director field. However, in our surface-responsive system, this complex dependence of light polarization on twisted director configurations does not degrade the optical sensitivity of the system but rather provides a diverse set of feedback mechanisms responsible for the formation of a large variety of light-driven dynamic and static patterns (Figs. 2-5 and 7).

Our photo-responsive self-patterning system can be maintained away from the equilibrium, resulting in the long-term dynamic patterns (Figs. 2-5 and 7), which only require low-intensity blue or ultraviolet light illumination to run for days and longer. This behavior is different from that of the chemical reaction diffusion systems, which slowly progress toward the thermodynamic equilibrium. Importantly, unlike the chemical systems exhibiting dynamic Archimedes spirals and other patterns, we can exquisitely control the speed of the propagating waves (Fig. 4) just by changing intensity of illumination light or by varying spectral composition of this light (e.g. using blue vs. ultraviolet, vs. red light). Despite the visual resemblance with the dynamic Archimedes spirals induced by the rotating magnetic field in Meyer's system, our patterns also show several key differences in their behavior: (1) the rates of counter-rotating spirals are practically the same in our patterns but different in Meyer's (with the difference between them slightly dependent on the spatial location of the pattern where the measurement is done and typically less than 10%, as seen from Fig. 2); (2) being induced in the bulk of homeotropic cells, Meyer's dynamic Archimedes spiral patterns exhibit motion of bulk solitons while our solitons emerge at surfaces with dynamically controlled DMR photoalignment layers; (3) in the very center of the spiral one expects having an umbilical defect in Meyer's magnetically driven Archimedes' spiral case, while we observe a boojum, which is due to the surface nature of our solitons; (4) since the magnetic field in Meyer's Archimedes' breaks the counter-clockwise vs. clockwise rotation symmetry, the stability and selected wavelengths of different dynamic Archimedes spirals in Meyer's case are not the same, unlike in our case, as light-induced patterns with different rotation directionality in our cells are kinetically and energetically indistinguishable; (5) our Archimedes spirals, unlike Meyer's [8–11], do not require dust particles or other inclusions to nucleate, which is because imperfections in the spatial patterns of the illumination light and the initial nonuniform states of the DMR monolayer can have the same effect, although physical imperfections can be responsible for this too.

In addition to dynamic patterns in the LC solitonic director structures and in molecular orientation patterns within the DMR self-assembled monolayers, we find that there is also self-patterning of the polarization state of outgoing light after traversing the LC cell. This can be clearly seen from the polarizing optical micrographs (Figs. 2, 4, 5, and 7) taken between crossed polarizers and especially the ones taken between the crossed polarizers with and additional phase retardation plate [Fig. 2(b)]. In the latter case, the different colors of the two twisted spatially-inter-winding domains within the optical micrographs indicate that the spiraling domains have orientations of polarization ellipses at rather large angles >90° with respect to each other. The analysis of polarizing optical micrographs of the patterns obtained without and with phase retardation plates (Figs. 2-5 and 7) shows that the self-patterning of LC twist domains and solitons is accompanied not only by self-patterning of orientationally

#231579 - $15.00 USD Received 2 Jan 2015; revised 4 Feb 2015; accepted 4 Feb 2015; published 12 Feb 2015

ordered structures in DMR monolayers but also by several types of optical dynamic patterns in terms of light's intensity, polarization state, and interference colors, all emerging from light's interaction with the dynamic structures of the director field in the LC film and polarizing optical elements (polarizer and wave plate) used in conjunction with it. It is fundamentally interesting that Archimedes spirals and other complex dynamic patterns in organization of matter and light can emerge from a spatially uniform and constant in time linear polarization of illumination light upon its interaction with the photoresponsive soft-matter system comprising a thin LC film and azobenzene self-assembled monolayer.

5. Conclusion

To conclude, we have developed a light-driven dynamic pattern-forming soft matter system that gives rise to non-equilibrium configurations and patterns in both matter and light. This self-patterning is enabled by a strongly polarization-sensitive nonlinear optical response due to an azobenzene-based alignment layer and a feedback mechanism through which the polarization state is controlled by twisted birefringent LC structures, and vice versa. A large diversity of dynamic patterns, including propagating Archimedes spiral waves, form as a result of this strong complex light-matter interaction. Similar to chaos theory [1], weak perturbations in the initial conditions of this system lead to dramatic changes in terms of the non-equilibrium dynamic behavior. This light-driven tunable pattern dynamics in LCs may provide an interesting model system of nonequilibrium biological phenomena, such as morphogenesis [1,2]. Although our modeling qualitatively describes observations, more detailed mathematical models of these phenomena themselves are needed and will be of great theoretical interest, potentially providing insights into their analogies and differences with respect to Turing instability and other nonequilibrium theories [1,2]. One possible interesting direction for the future studies is to characterize Lyapunov exponents under different pattern-forming conditions in our anisotropic soft matter system. Finally, to the best of our knowledge, the described observations provide the only experimentally documented example where low-intensity (even ambient) light-matter interaction can yield dynamic self-patterning in the matter itself and in polarization, color, and intensity of light interacting with it. From the practical applications viewpoint, this system may provide the means for generating dynamic patterns of time-varying polarization and dynamic optical vortices needed for singular optics uses, as well as various light-driven micro-machines. By combining the structural diversity of our patterns with polymerization of various photo- and thermally-responsive LC polymers and elastomers, one can potentially realize novel types of dynamic changes of thin film topography controlled by weak external stimuli and light [32]. The dynamic Archimedes spiral patterns may be also useful in digital light processing [1,2].

Acknowledgements

We acknowledge support by the National Science Foundation Grant DGE-0801680 (A.M., through a COSI IGERT fellowship) and also partial support by the U.S. Department of Energy, Office of Basic Energy Sciences, Division of Materials Sciences and Engineering, under the Award ER46921 (A.M. and I.I.S.).

#231579 - $15.00 USD Received 2 Jan 2015; revised 4 Feb 2015; accepted 4 Feb 2015; published 12 Feb 2015